Impedance and Admittance Waveguide Inverter Applications: A Practical Sub-Terahertz Region Tolerance Analysis for Large-Scale Production

Chad Bartlett, *Member, IEEE*, Jens Bornemann, *Life Fellow, IEEE*, Fynn Kamrath, *Graduate Student Member, IEEE*, and Michael Höft, *Senior Member, IEEE*

***Abstract*— This work presents an in-depth analysis of the four most basic waveguide inverter types; *E*-plane irises, *E*-plane stubs, *H*-plane irises, and *H*-plane stubs. A thorough investigation and tolerance analysis of fourth-order filters, which are comprised of each of the inverter types, is undertaken in order to identify and communicate sensitivity, fabrication practicality, and special considerations for the mass production of waveguide filters operating in the sub-terahertz (THz) region, while, in addition, aims to resolve open questions with regards to the direct comparison of performance between each of the filter profiles. A total of forty filters are fabricated and measured for operation at 267.5 GHz with a 5.6% fractional bandwidth. The results are detailed and a yield summary is presented for an 80% bandwidth criteria with return loss operating conditions at 18 and 20 dB. The highest product yield is found to be of the stub filter types, that being 90% each when a 20-dB criteria is applied, while the lowest yield is of the *H*-plane iris filter type, that being 50% when a 20-dB criteria is applied. The measured results indicate that both of the stub-type filter profiles also result in a lower insertion loss when compared to the iris-type designs. An additional evaluation is provided at the end of this article with the production of another six *H*-plane iris-type filter prototypes with per-contra cutting planes in order to discuss and contrast the measured results of *E*- and *H*-plane cutting profiles and their respective relationship to the milling depth and attainable aspect ratio in sub-THz applications.**

***Index Terms*— Admittance inverters, filter design, high-precision milling, impedance inverters, *J*-band, manufacturing, sub-terahertz (THz), THz, tolerance analysis, waveguide filters.**

I. Introduction

MANUFACTURING capabilities, in hand with technological advancements, must be rigorously tested, reinvented, and explored. In order to reach viable and reliable production, whether subtractive or additive in nature, new perspectives must be examined for overcoming the inherently miniaturized dimensions and sensitivity of components within the terahertz (THz) and sub-THz regions.

Tolerance analyses and parametric studies are often used in the testing and validation of individual designs, and, at very high frequencies, can allow for the selection of alternate dimensions as a means of avoiding structures that are overly sensitive to deviations from the desired dimensions and still fall within the bounds of manufacturers' stated tolerance values. In this manner, designers can aim to counteract the degradation of the desired response by selecting a physical structure and/or characteristic response that is capable of tolerating small fabrication errors.

In the case of high-frequency cavity filters, a compelling study provided by Bornemann et al. [1] investigated many different structures as a means of determining the impact of cross-couplings on the passband response. The conclusion from this work suggests that the addition of cross-couplings do not impact the passband sensitivity in any meaningful way and that the fractional bandwidth (FBW) has a higher impact on the filter response. Studies provided in [2] investigated the fabrication accuracy and repeatability of silicon-micromachined filters using the deep reactive ion etching (DRIE) technique where a yield of approximately 50% was demonstrated. However, one of the major difficulties in this production method lies with reliability and repeatability in the assembly and alignment process of the chips in multilayer device design. In regards to other waveguide-based filter structures that are beyond the microwave region (i.e., >30 GHz), works, such as [3], [4], [5], [6], [7], [8], and [9], have demonstrated unique designs accompanied by studies on the effect of dimensional sensitivities up to 330 GHz; however, no meaningful determinations on the sensitivities of the cutting planes have been determined.

Most often, dimensional analyses are provided for a particular design and lack a more global comparison to other relative or suitable structures, or moreover, lack a solution for reducing the sensitivity of the component at hand. Albeit, an interesting solution provided in [10] proposes a redistribution of the poles within the passband to take on the form of a "dome" shape, which is shown to ultimately

Manuscript received 3 July 2023; revised 18 January 2024; accepted 6 February 2024. Date of publication 8 February 2024; date of current version 15 April 2024. This work was supported by the European Union's Horizon 2020 Research and Innovation Programme through the Marie Skłodowska-Curie Grant under Agreement 811232-H2020-MSCA-ITN-2018. Recommended for publication by Associate Editor X. Gu upon evaluation of reviewers' comments. *(Corresponding author: Chad Bartlett.)*

Chad Bartlett, Fynn Kamrath, and Michael Höft are with the Department of Electrical and Information Engineering, Kiel University, 24143 Kiel, Germany (e-mail: cbartlett@ieee.org; flk@tf.uni-kiel.de; mh@tf.uni-kiel.de).

Jens Bornemann is with the Department of Electrical and Computer Engineering, University of Victoria, Victoria, BC V8W 2Y2, Canada (e-mail: j.bornemann@ieee.org).

Color versions of one or more figures in this article are available at https://doi.org/10.1109/TCPMT.2024.3364509.

Digital Object Identifier 10.1109/TCPMT.2024.3364509

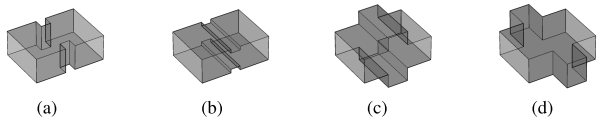

Fig. 1. Basic forms of waveguide inverters: (a) H-plane (inductive) iris; (b) E-plane (capacitive) iris; (c) E-plane (capacitive) stub; and (d) H-plane (inductive) stub. Adapted from [12].

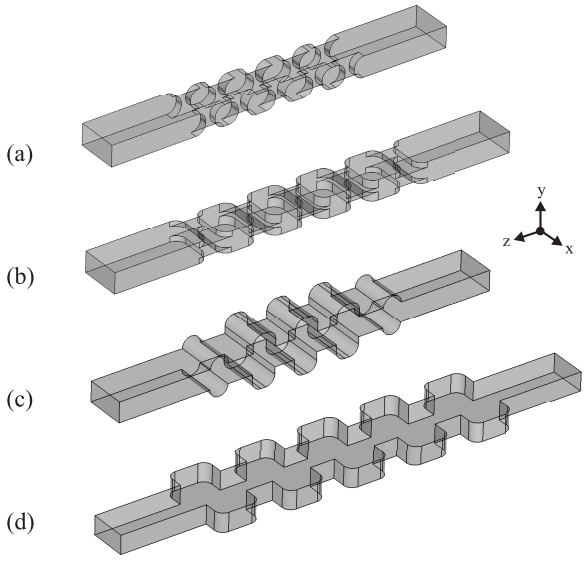

Fig. 2. Simulated vacuum-shell structures of fourth-order waveguide filters using either all-impedance or all-admittance inverters. The models are based on the form of: (a) H-plane (inductive) iris; (b) E-plane (capacitive) iris; (c) E-plane (capacitive) stub; and (d) H-plane (inductive) stub. Relative sizes are shown for comparison. Overall length of each filter body from iris-to-iris is: (a) 3.598 mm; (b) 4.946 mm; (c) 4.250 mm; and (d) 6.992 mm.

reduce sensitivities in the fabrication process by minimizing the return loss ripple at the passband edges. This technique can be used quite universally since the method does not depend on the type of manufacturing technology. In the case of high-production manufacturing, whether the selected fabrication method is subtractive or additive in nature, individual technology platforms have their own inherent traits and manufacturing challenges that need to be understood, for instance, a scaling factor can be used to compensate the shrinkage and expansion of resin during the curing process of stereolithography 3-D printing (e.g., [11]).

In this work, we provide an assessment of the most basic coupling inverters used for empty-cavity waveguide filters. The four inverter types are illustrated in Fig. 1. The structures in Fig. 1(a) and (b) take the form of E-plane and H-plane iris (impedance) inverters, and the structures in Fig. 1(c) and (d) take the form of E-plane and H-plane stub (admittance) inverters. In the vast majority of cases, inductive and capacitive irises are used for the realization of filter networks, where a wide variety is explored in [13]. Although less common, stub-type inverters can be used as an effective substitute as the coupling means between two resonators. These stub-based coupling schemes are rarely demonstrated as all-admittance inverter type filters ([12] and [14]) and usually appear in combination with impedance inverters as to improve the rejection-band characteristics, for example, [15] and [16].

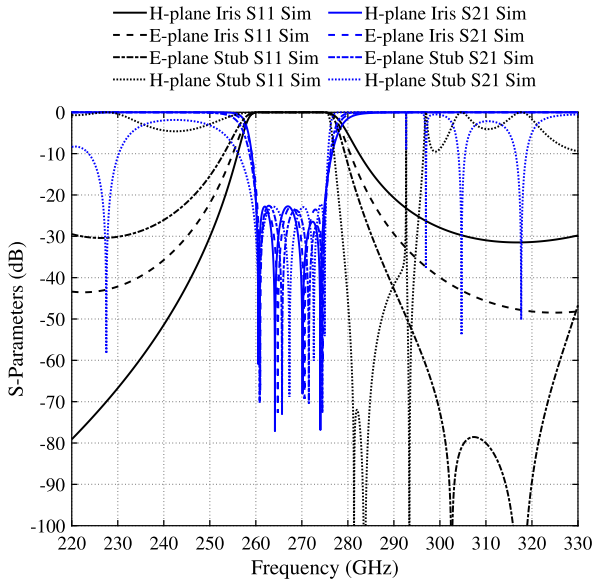

Fig. 3. Comparison of the simulated lossless S-parameters for each of the fourth-order filters depicted in Fig. 2.

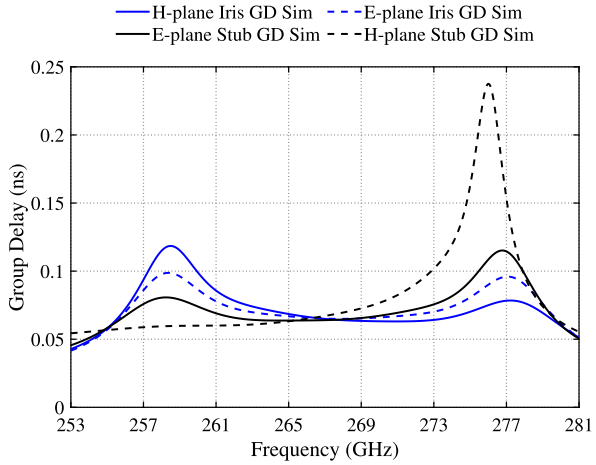

Fig. 4. Comparison of the simulated group delay for each of the fourth-order filters described by Figs. 2 and 3.

Although the evident shortcomings of over-moding in stub-type filters can degrade the rejection region and increase the physical size of the desired filter, there may be cases where designers can benefit from the use of an alternative topology or characteristic response, especially when producing high-performance systems that require minimal insertion loss and minimal offset from the desired center frequency. Furthermore, the failure to meet the desired specifications can also require tedious redesign and production iterations.

In this regard, we aim to investigate and resolve the following questions that have not yet been addressed in the literature in regards to the use of inverter types and their application in very high-frequency designs.

1) Is a milling tolerance range of ± 5 μm adequate for sub-THz filter design, and subsequently, what is an appropriate return loss margin for mass production?
2) Is there a combination of all E-plane/H-plane/iris/stubs that is meaningfully more robust to milling inaccuracies?

3) Given similar passband specifications, what is the average measured insertion loss of each all-impedance and all-admittance inverter filter design?
4) Given similar passband specifications, is there a meaningful variation in terms of physical size between each of the designs?

To this end, we present the following analysis on the four basic impedance and admittance waveguide-inverter types. Four different filters are designed with either all-impedance or all-admittance inverters, each of which having similar passband specifications and operating as fourth-order filters in the sub-THz region. The four filter designs are detailed and their respective S-parameters and group-delay responses are compared and contrasted. A tolerance analysis is provided for each design with a range of ± 5 μm. In order to verify the designs, forty filters are manufactured and again compared. The results are communicated as a qualitative study on the impact of waveguide inverter types and tabulated as a yield percentage with a pass or fail criteria. An additional section is provided as a supporting evaluation of the results by producing another six filters that are again compared and tabulated. Forty-six filters were analyzed in total.

II. Impedance and Admittance Filters

In order to investigate the questions raised in Section I, an analysis of the four basic waveguide inverters is undertaken with specifications in the sub-THz region where the network synthesis follows from the full-wave edge-conditioned-based coupled-integral-equations technique (CIET), which can be reviewed in [17], [18], and [19]. Specifically, the WR-3 waveguide region covers the frequency range from 220 to 330 GHz. This range is selected for its exceptionally miniaturized size requirements as well as the considerable amount of research interest that stems from the evolution of high-speed communications, Internet of Things (IoT), and satellite communications [20], [21].

In this regard, four different types of fourth-order filters are designed with similar FBWs of approximately 5.6% and centered around 267.5 GHz. In this manner, a range from 260 to 275 GHz is covered throughout each passband. Each of the filters are designed as either all-impedance or all-admittance inverter-type filters and are depicted in Fig. 2(a)–(d) in vacuum-shell format. Fig. 2(a)–(d) is portrayed with relative sizes to one another for visual reference with their final lengths (in mm) provided in the image caption. All four filters have been designed with a WR-3 waveguide specification in mind for either milling along the E-plane or H-plane, and have been specified with 0.2-mm cutting radii. The simulated lossless S-parameter results are depicted in Fig. 3. In this image, the filter responses can be compared to one another, where the most prominent differences arise with the introduction of frequency-dependent transmission zeros and spurious modes stemming from the all-admittance filter designs, and most related to the large H-plane stubs of the filter shown in Fig. 2(d). It is important to note that all of the structure's dimensions, including the waveguide housing, have all been rounded to three decimal places to enable precise and accurate milling. In this manner, small deviations arise in the return loss ripple; however, each return loss response is below 22 dB in order to give a 2-dB passband margin in the simulated lossless case, and a 3-dB margin in the simulated lossy case. In addition to Fig. 3, the simulated group-delay functions are given in Fig. 4. It is noteworthy to observe the differences in the group-delay functions and that the most symmetric function around 267.5 GHz is the E-plane iris-type filter, as shown in Fig. 2(b), where each of the peaks remains below 0.1 ns.

III. Tolerance Analysis

In order to assess the structures outlined in Fig. 2, a tolerance analysis is run with random points within ± 5 μm for 100 simulation runs with an effective conductivity set to 1.8 MS/m [7]. A variation of ± 5 μm has been selected as a realistic dimensional target that is capable of most modern high-end computer numerical control (CNC) milling machines. With the error boundary defined, the simulated errors are randomly chosen within that range and added to the structure's dimensional profile for simulation. The random error for each of the filter's dimensions is the result of a uniform distribution where the summation of the errors results in a normally distributed function. Fig. 5 depicts each of the filter goals with an overlay of the simulated tolerance analysis S-parameters and allows for a predictive baseline of the expected outcome of the fabricated filters. It can be noted that for this analysis, the dimensions of the structures were varied randomly; however, both the corner radii and small misalignments (associated with the assembly along the relative cutting planes) were not considered. Although these deviations were not taken into account, the dimensional variations that are applied to the ideal models still allow for a comprehensive overview of the effects on the desired S-parameter response.

The simulations are run for the full J-band range. The critical dimension correlation follows standard filter theory where the resonator dimensions primarily affect the center frequency position, while the iris dimensions primarily affect the filtering bandwidth. Studying Fig. 5, it can be noted that the simulations do not significantly deviate in center frequency position or bandwidth, rather, the cumulative effects pose significant degradation of the in-band return loss level. Even though a 3-dB margin has been given to each of the designs, the S-parameter variations indicate a return loss worse than the desired 20-dB level. Only in Fig. 5(d)—the H-plane stub-type filter—a close to 20-dB margin can be observed in the lower end of the passband, while the upper end indicates a high sensitivity that causes the return loss to degrade from the 20-dB specification.

IV. Fabrication and Measurement

For the fabrication of each of the filters, brass has been selected as the cutting material due to its machinability and final surface finish. For each of the four filter types, a set of ten filters was milled within the same brass block in a 1×10 fashion. By manufacturing the ten filters in the same metal block, errors associated with alignment as well as brass

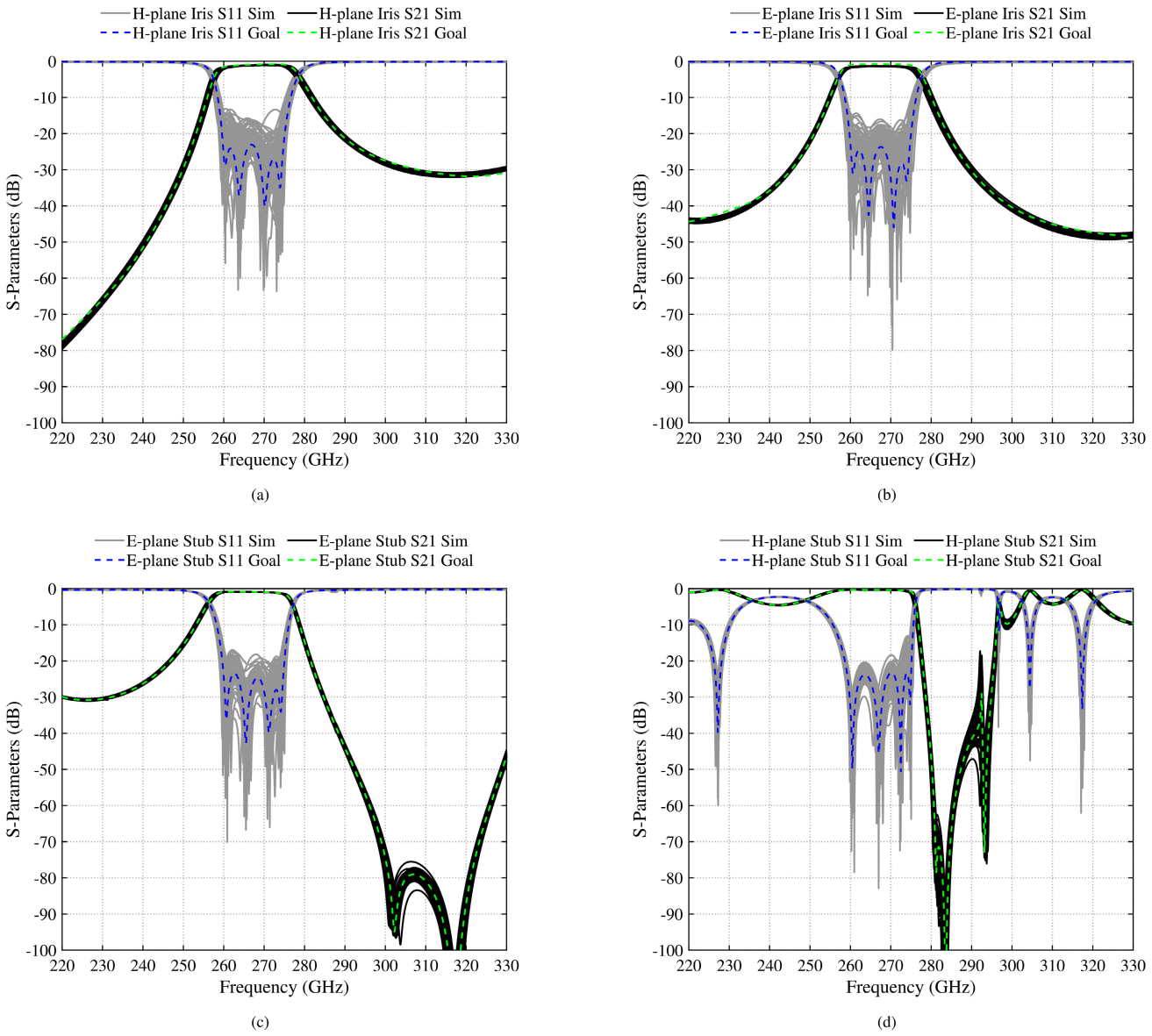

Fig. 5. Simulated S-parameter goal and tolerance analysis of the prototype filters. (a) H-plane (inductive) iris filter. (b) E-plane (capacitive) iris filter. (c) E-plane (capacitive) stub filter. (d) H-plane (inductive) stub filter.

conductivity variations can be minimized. This allows for a more accurate assessment of the realized milling profiles. For each of the filter designs, the radii were set to 0.2 mm, while each of the 1×10 filter banks was milled in either a split E-plane or split H-plane format according to their respective filter designs and achievable aspect ratio of the milling tool, that being an E-plane cut for the H-plane iris and E-plane stub filters, and an H-plane cut for the E-plane iris and H-plane stub filters. Standard UG-387/U flanges are used to feed each of the filters; no additional precision dowels or rings [22] were used for waveguide port alignment. As noted in Section II, the dimensions of the filter structures, including the waveguide housing, have been rounded to three decimal places to enable precise and accurate milling. In Fig. 6, an example of a 1×10 filter bank is shown along the cutting plane, along with a laser-microscope view of one of the internal H-plane stub structures. The surface roughness S_a of the component is measured to be approximately 0.7 μm.

Once each of the filter banks was produced, a Rohde & Schwarz ZVA67 with WR-3 converters was calibrated using the thru-reflect-line (TRL) method and employed to measure each of the forty filters. This procedure was completed in one sequence, and all of the filters were tested at one time in order to avoid any possible errors that could stem from multiple calibrations at different periods of time. An image of the H-plane stub filter connected to the test bed is provided in Fig. 6. The measured results are given in Fig. 7(a)–(d) with the overlay of all ten filter measurements in each of the plots. The red dashed line is used to indicate an 18-dB operational return loss between 261.5 and 273.5 GHz (80% of the passband range). It can be noted that no Au (gold) or Ag (silver) coatings have been applied to enhance the measured performances.

In general, all forty filters demonstrate accurate measurements around the specified center frequency without any major deviations; however, it can be noted that some of the measured profiles fall outside of the predicted tolerance-analysis profiles

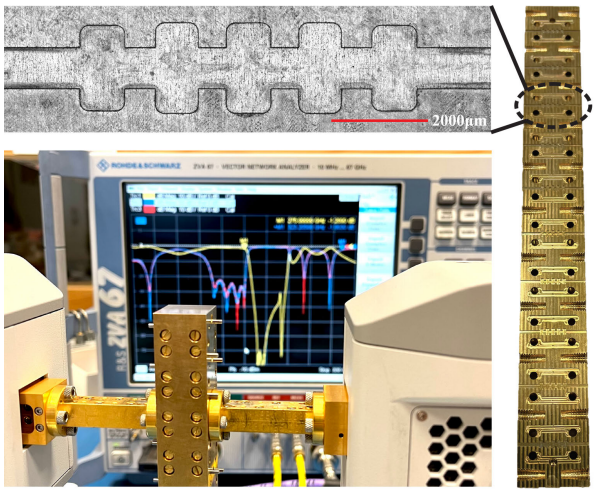

Fig. 6. Fabricated prototypes under test. The top-left exhibits a laser-microscope image of a single H-plane stub filter, the bottom-left depicts the filter connected to the test bed, and the right-side image is a camera image of the internal structures of the 1×10 filter block before final assembly.

in Fig. 5. This suggests several points of error to be considered during assessment and valuation, such as: possible manufacturing errors at the limits or beyond ± 5 μm, small misalignments in assembly along the E-plane or H-plane cut, localized gaps in assembly, and sufficient modeling accuracy (meshing, finite integration technique (FIT)/finite-element method (FEM), etc.). Nevertheless, the measurements are sufficient for prototyping purposes and a more in-depth evaluation on the subtleties of the responses will be made in Section V.

V. Assessment and Valuation

In Section IV, the measurements of all the filters were presented. Conventionally, all of the filters would be regarded to have good measurements throughout the 220–330-GHz region, and predict the behavior of each of the four filter designs. However, in this section, we assess the measured results more in depth as a means of providing a more qualitative discussion and outcome. It should be noted that no measurement results at any point are subject to "over-calibration" (positive insertion loss or return loss values), which would dramatically affect the outcome of a study on passive devices.

Table I provides a summary on the assessment of each filter type. The average insertion losses throughout the targeted frequency range (80% of the 15-GHz passband at 267.5 GHz) of each of the filter types reveal that the E-plane and H-plane iris filter types are in the range of 1.18–1.40 dB, and 1.04–1.46 dB, respectively, while the E-plane and H-plane stub filter types are in the range of 0.70–0.92 dB and 0.80–1.18 dB, respectively. Using the 80% targeted frequency range and 20-dB return loss level as a metric of qualitative yield, the highest yields are found to be of the E-plane iris, E-plane stub, and H-plane stub-type filters, with 80%, 90%, and 90%, respectively, while the lowest yield is the H-plane iris-type filter with 50%. Relaxing this metric to a reasonable return loss level of 18 dB, the H-plane iris filter's yield is improved to 80%.

It is interesting to notice from Table I that both the E- and H-plane iris profiles result in a higher average insertion loss than the stub-type profiles. This difference is indicated to be a product of the stub-type profiles having an increased inverter volume that does not impede the standard (i.e., WR-3) waveguide dimensions. Moreover, the H-plane iris filters result in the lowest yield, that being 50% and 80%, when using the 20- and 18-dB rejection criteria, respectively. On the consideration of these dramatic differences in a 20-dB yield criteria, one may examine the sensitivities of each filter exhibited in Fig. 5 or criticize the variations of the simulated return loss ripple at the 23-dB level, in an attempt to correlate some of the errors to the yield; however, except for the lower passband simulations of Fig. 5(d), the comparative sensitivities between each filter is difficult to characterize in a meaningful way at such high frequencies; this is especially true considering that variation in the return loss ripple is even subject to the simple round off of dimensional values to three decimal places for practical milling. Notwithstanding, the lower yield with regard to iris-type filter return loss criteria may also be indicative of the irises inherent roll of impeding the standard waveguide dimensions and causing reflections. These results suggest that a 3-dB margin may still not be sufficient for achieving high-yield production and a greater margin should be accounted for. For instance, with an 18-dB criteria (signal reflection being 1.58%), a 6-dB margin would be more appropriate.

On comparison of the cutting planes with the average insertion loss values, neither attribute seems to definitively hinder or aid the measurements. The E-plane cuts do have a slightly lower insertion loss; however, this may be attributed to other factors such as the design profiles rather than the cutting plane. This is interesting to note because microwave component designers generally aspire to use an E-plane cutting profile to reduce passive intermodulation effects, as well as limit the effect of mechanical discontinuities disrupting the surface current distribution. For a more direct comparison of the cutting plane effects on the filters, as well as the effects related to the contrast in milling depths and aspect ratio, a related study on the cutting profile is more appropriate. This contrast in milling depth is illustrated in Fig. 8, where it can be observed that the centered H-plane cutting profile in a block is half the depth ($b/2$) of the centered E-plane cutting profile depth (b). In low-frequency design profiles, this subtle observation may have been irrelevant due to comprehensive sizeable milling tools available; however, this can lend itself to ramifications in sub-THz or THz manufacturing where the design profile, milling tools, and aspect ratios must be seriously considered and may result in the difference between achieving or failing the required specifications of stringent applications. In order to investigate this supposition further, Section VI has been added as a supporting study where a 1×6 H-plane iris filter block is manufactured and assessed.

VI. H-Plane Iris Cutting Profile Evaluation

In Section V, it has been observed that the stub-type filter profiles exhibit a lower average insertion loss than the

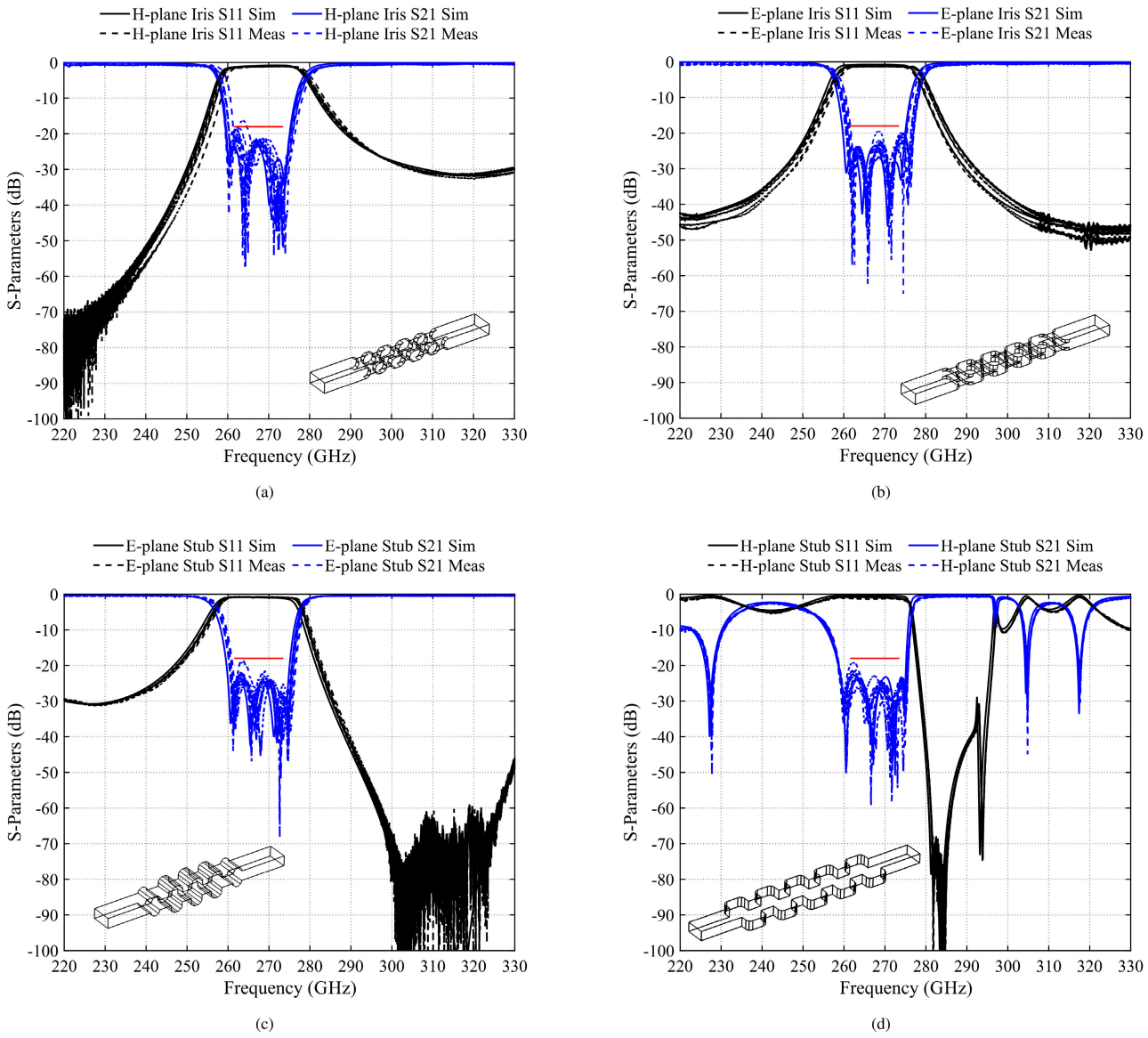

Fig. 7. Simulated versus measured S-parameters the prototype filters. There are ten filters measured of the: (a) H-plane (inductive) iris filter; (b) E-plane (capacitive) iris filter; (c) E-plane (capacitive) stub filter; and (d) H-plane (inductive) stub filter. The red boundary lines indicate the 18-dB return loss level.

iris-type filter profiles (review Table I), and on comparison of the cutting planes with respect to insertion loss or return loss, only minor distinctions can be made. However, it is often desired for components to be fabricated with a centered E-plane cut, or even monolithically, to avoid disruption of the surface currents. In this respect, we evaluate the measured results and yield of one of the filter profiles in order to understand the significance/consequence of the milling depth and aspect ratio that is associated with the centering of the cutting profile (i.e., centered E-plane or centered H-plane) at sub-THz frequencies. In order to investigate this E-plane versus H-plane supposition, a 1×6 filter block has been designed and assessed similar to the fabrication and measurement techniques that have been outlined in Section IV.

A. H-Plane Iris Filter Designs

For this study, the H-plane iris-type filter [Fig. 2(a)] has been selected due to being one of the most common and well-known waveguide filter profiles. Three of the filters are manufactured with an H-plane cutting profile, and another three are manufactured with an E-plane cutting profile. The lossless simulated results and profile of each filter body are shown in Fig. 9. The target center frequency and bandwidth remain as 267.5 and 15 GHz, respectively, and the simulated responses indicate a very good match, especially in regards to the return loss ripple. Each filter profile has similar attributes, such as 0.2-mm-radius corners and 2.0-mm iris lengths. This has been done in order to limit the variations and geometric differences in the filter profiles. The prototype block is again manufactured in brass, and no additional conductive plating is applied. Fig. 10 illustrates the simulated group delay of each of the filters. Fig. 11 depicts the laser-microscope images and depth profiles of an H-plane cut and an E-plane cut filter in the 1×6 block.

B. H-Plane Iris Filter Evaluation

The measurements of the 1×6 filter block are presented in Fig. 12(a) and (b). Using the same metrics that have

TABLE I
SUMMARY OF THE ALL-IMPEDANCE AND ALL-ADMITTANCE INVERTER-TYPE FILTER YIELD (TEN PROTOTYPES EACH)

Filter Profile	Cutting Plane (Centered)	Target Smd-XZ† (μm)	Avg. IL‡ (dB)	20 dB RL Pass/Fail (Yield)	18 dB RL Pass/Fail (Yield)
H-Plane Iris	E-Plane	Iris Length 200	1.04 - 1.46	5/5 (50%)	8/2 (80%)
E-Plane Iris	H-Plane	Iris Length 300	1.18 - 1.40	8/2 (80%)	9/1 (90%)
E-Plane Stub	E-Plane	Stub End to WG 196.5	0.70 - 0.92	9/1 (90%)	10/0 (100%)
H-plane Stub	H-plane	Stub End to WG 464	0.80 - 1.18	9/1 (90%)	10/0 (100%)

†Smd = Smallest milled dimension of the X (width) and Z (length) directions, ‡Average insertion loss range over the target frequency range, WG = Waveguide.

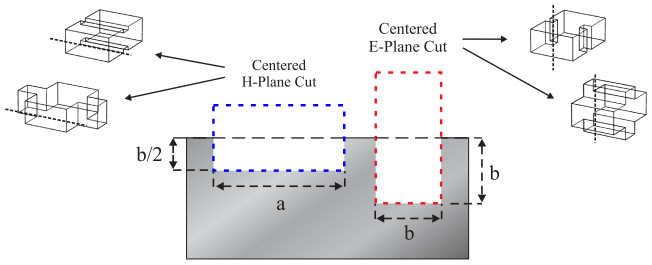

Fig. 8. Comparison of the centered cutting profiles for H-plane and E-plane filter designs.

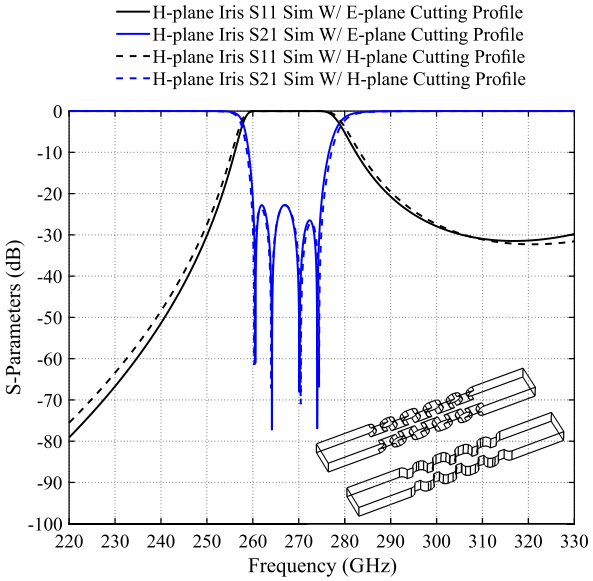

Fig. 9. Comparison of the simulated lossless S-parameters for the fourth-order H-plane iris filters with H-plane and E-plane cutting profiles.

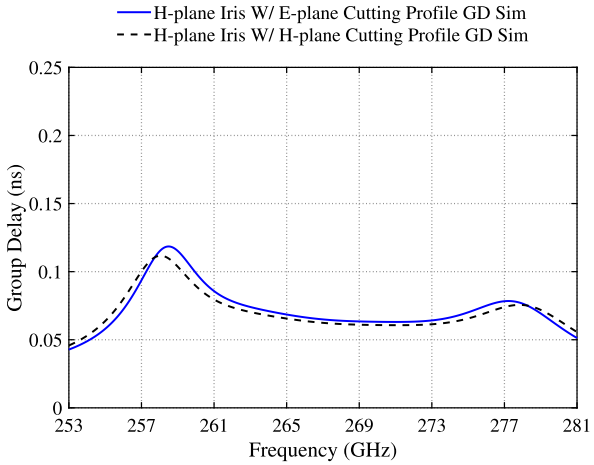

Fig. 10. Comparison of the simulated group delay for each of the fourth-order filters described in Fig. 9.

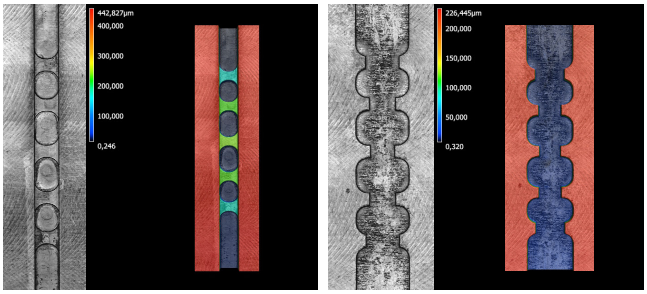

(a) (b)

Fig. 11. Fabricated 1 × 6 prototype block samples. Each image exhibits a laser microscope and depth profile of an: (a) E-plane cut H-plane iris filter and (b) H-plane cut H-plane iris filter.

been applied in Section V (80% of the 15-GHz passband at 267.5 GHz), the average insertion loss in the targeted passband of the E- and H-plane cutting profiles that are presented in Fig. 12 are found to be on the ranges of 0.95–1.41 dB and 1.50–1.86 dB, respectively. Using the 20-dB return loss yield criteria, the E- and H-plane cutting profiles render a result of 100% and 33.3% yield, while the 18-dB return loss criteria results in 100% yields for both profiles. A summary of these results is presented in Table II. From these results, along with the previous results presented in this article, the H-plane iris filters with E-plane cuts show to have similar average insertion loss values, that being, 1.04–1.46 dB from Table I and 0.95–1.41 dB from Table II, demonstrating continuity of results. Upon comparing the H-plane iris filters based on their respective cutting planes, the E-plane cutting profile has approximately 0.5 dB lower insertion loss even though the E-plane cut requires a higher aspect ratio. Furthermore, it is interesting to note that the return loss ripple does not rise above 20 dB for this profile and also suffers from a small center frequency shift in the passband. This indicates that the E-plane cut is the preferred method even at the risk of using higher aspect-ratio milling tools.

TABLE II
SUMMARY OF THE ALL-IMPEDANCE INVERTER-TYPE FILTER YIELD (SIX H-PLANE IRIS PROTOTYPES)

Filter Profile	Cutting Plane (Centered)	Target Smd-XZ† (μm)	Avg. IL‡ (dB)	20 dB RL Pass/Fail (Yield)	18 dB RL Pass/Fail (Yield)
H-Plane Iris	E-Plane	Iris Length 200	0.95 - 1.41	3/0 (100%)	3/0 (100%)
H-Plane Iris	H-Plane	Iris Length 200	1.50 - 1.86	1/2 (33.3%)	3/0 (100%)

†Smd = Smallest milled dimension of the X (width) and Z (length) directions, ‡Averaged insertion loss range over the target frequency range.

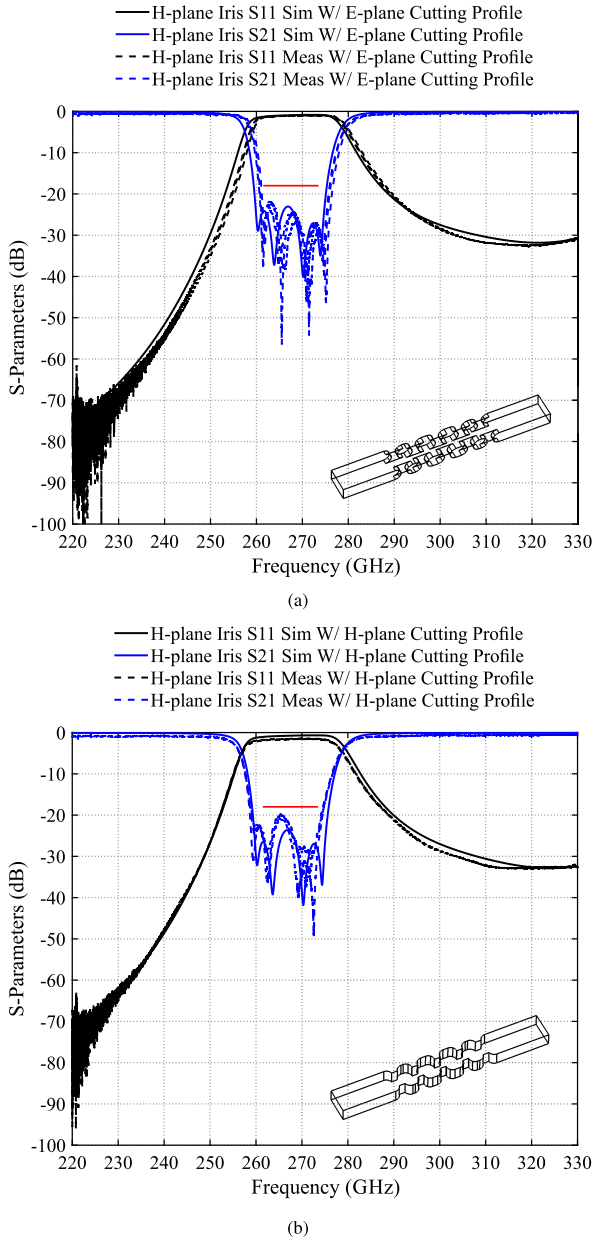

Fig. 12. Simulated versus measured S-parameters of the supporting evaluation prototype filters. There are three filters measured of the H-plane iris type with an: (a) E-plane and (b) H-plane cutting profile. The red boundary lines indicate the 18-dB return loss level.

VII. CONCLUSION

An in-depth analysis of four waveguide filters comprised of four fundamental inverter models has been presented in the J-band for 267.5-GHz operation. Each of the models are described and contrasted while a tolerance analysis of each model demonstrates the typical achievable results within a ± 5-μm variation in order to further investigate and resolve underlying questions on the use of fundamental inverter types. An assessment of the yield has been obtained by manufacturing ten of each type of filter with similar passband characteristics. A 6-dB return loss margin with an estimated effective conductivity of 1.8 MS/m (at least in the WR-3 range) has been indicated as a good design guideline in order to overcome dimensional inaccuracies due to the milling process. A discussion and comparison on the overall filter lengths and robustness to dimensional inaccuracies has been presented. Although the H-plane stub-type filter produces spurious modes within the frequency band of interest due to over-moding, the highest yield and lowest average insertion loss values were achieved and starkly contrasted from the H-plane iris filter, which resulted in the lowest yield.

REFERENCES

[1] J. Bornemann, U. Rosenberg, S. Amari, and R. Vahldieck, "Tolerance analysis of bypass-, cross- and direct-coupled rectangular waveguide band-pass filters," *IEE Proc. Microw., Antennas Propag.*, vol. 152, no. 3, p. 167, Jun. 2005, doi: 10.1049/ip-map:20041158.

[2] O. Glubokov, X. Zhao, J. Campion, B. Beuerle, U. Shah, and J. Oberhammer, "Investigation of fabrication accuracy and repeatability of high-Q silicon-micromachined narrowband sub-THz waveguide filters," *IEEE Trans. Microw. Theory Techn.*, vol. 67, no. 9, pp. 3696–3706, Sep. 2019, doi: 10.1109/TMTT.2019.2926244.

[3] J. Xu, J.-Q. Ding, Y. Zhao, and J.-X. Ge, "W-band broadband waveguide filter based on H-plane offset coupling," *J. Infr., Millim., THz Waves*, vol. 40, no. 4, pp. 412–418, Apr. 2019, doi: 10.1007/s10762-019-00571-7.

[4] Y. Xiao, T. Li, and H. Sun, "A novel W-band waveguide bandpass filter based on nonresonating nodes," in *Proc. IEEE Int. Conf. Microw. Millim. Wave Technol. (ICMMT)*, Jun. 2016, pp. 833–835, doi: 10.1109/ICMMT.2016.7762458.

[5] F. Teberio et al., "Waveguide band-pass filter with reduced sensitivity to fabrication tolerances for Q-band payloads," in *IEEE MTT-S Int. Microw. Symp. Dig.*, Jun. 2017, pp. 1464–1467, doi: 10.1109/MWSYM.2017.8058897.

[6] A. Sami et al., "Robust tolerance design of bandpass filter with improved frequency response for Q-band satellite applications," *IEEE Microw. Wireless Compon. Lett.*, vol. 31, no. 11, pp. 1183–1186, Nov. 2021, doi: 10.1109/LMWC.2021.3090218.

[7] D. Miek, F. Kamrath, P. Boe, and M. Höft, "WR-3 band waveguide filter tolerance analysis and surface metallization comparison," *J. Infr., Millim., THz Waves*, vol. 41, no. 12, pp. 1576–1590, Aug. 2020, doi: 10.1007/s10762-020-00735-w.

[8] D. Miek, C. Bartlett, F. Kamrath, P. Boe, and M. Höft, "Investigation of the cutting plane and tolerance analysis of cross-coupled W-band waveguide filters with multiple transmission zeros by source to load cross-coupling," *Int. J. Microw. Wireless Technol.*, vol. 14, no. 3, pp. 369–378, Apr. 2022, doi: 10.1017/s1759078721000957.

[9] C. Bartlett, M. M. Gohari, O. Glubokov, J. Oberhammer, and M. Höft, "Compact triangular-cavity singlet-based filters in stackable multilayer technologies," *IEEE Trans. THz Sci. Technol.*, vol. 12, no. 5, pp. 540–543, Sep. 2022, doi: 10.1109/TTHZ.2022.3191237.

[10] A. B. Jayyousi, M. J. Lancaster, and F. Huang, "Filtering functions with reduced fabrication sensitivity," *IEEE Microw. Wireless Compon. Lett.*, vol. 15, no. 5, pp. 360–362, May 2005, doi: 10.1109/LMWC.2005.847713.

[11] C. Bartlett, D. Miek, F. Kamrath, D. Bruhn, and M. Hoft, "X-band 3D-printed metal-insert twist-component for bandpass filter applications," in *IEEE MTT-S Int. Microw. Symp. Dig.*, Nov. 2021, pp. 329–331, doi: 10.1109/imfw49589.2021.9642300.

[12] C. Bartlett, J. Bornemann, and M. Hoft, "3-D-printing and high-precision milling of W-band filter components with admittance inverter sequences," *IEEE Trans. Compon., Packag., Manuf. Technol.*, vol. 11, no. 12, pp. 2140–2147, Dec. 2021, doi: 10.1109/TCPMT.2021.3116220.

[13] G. L. Matthaei, L. Young, and E. M. Jones, *Microwave Filters, Impedance-matching Networks, and Coupling Structures*. Norwood, MA, USA: Artech House, Feb. 1980.

[14] Q. Wang and J. Bornemann, "Synthesis and design of direct-coupled rectangular waveguide filters with arbitrary inverter sequence," in *Proc. 16th Int. Symp. Ant. Technol. App. Electromag. (ANTEM)*, Jul. 2014, pp. 1–6, doi: 10.1109/ANTEM.2014.6887723.

[15] W. Menzel, F. Alessandri, A. Plattner, and J. Bornemann, "Planar integrated waveguide diplexer for low-loss millimeter-wave applications," in *Proc. 27th Eur. Microw. Conf.*, vol. 2, Jerusalem, Israel, Sep. 1997, pp. 676–680, .

[16] M. Salehi, J. Bornemann, and E. Mehrshahi, "Substrate-integrated waveguide band pass filters with frequency-dependent coupling elements," *Int. J. RF Microw. Comput.-Aided Eng.*, vol. 24, no. 2, pp. 237–242, Mar. 2014, doi: 10.1002/mmce.20754.

[17] S. Amari, J. Bornemann, and R. Vahldieck, "Accurate analysis of scattering from multiple waveguide discontinuities using the coupled-integral equations technique," *J. Electromagn. Waves Appl.*, vol. 10, no. 12, pp. 1623–1644, Jan. 1996, doi: 10.1163/156939396x00351.

[18] S. Amari, J. Bornemann, and R. Vahldieck, "Fast and accurate analysis of waveguide filters by the coupled-integral-equations technique," *IEEE Trans. Microw. Theory Techn.*, vol. 45, no. 9, pp. 1611–1618, Sep. 1997, doi: 10.1109/22.622929.

[19] J. Bornemann, U. Rosenberg, S. Amari, and R. Vahldieck, "Edge-conditioned vector basis functions for the analysis and optimization of rectangular waveguide dual-mode filters," in *IEEE MTT-S Int. Microw. Symp. Dig.*, vol. 4, Anaheim, CA, USA, Jun. 1999, pp. 1695–1698, doi: 10.1109/MWSYM.1999.780297.

[20] M. Ivashina, A. Vilenskiy, H.-T. Chou, J. Oberhammer, and M. N. M. Kehn, "Antenna technologies for beyond-5G wireless communication: Challenges and opportunities," in *Proc. Int. Symp. Ant. Propag. (ISAP)*, Oct. 2021, pp. 1–2, doi: 10.23919/ISAP47258.2021.9614381.

[21] W. Jiang, B. Han, M. A. Habibi, and H. D. Schotten, "The road towards 6G: A comprehensive survey," *IEEE Open J. Commun. Soc.*, vol. 2, pp. 334–366, 2021, doi: 10.1109/OJCOMS.2021.3057679.

[22] N. M. Ridler and R. A. Ginleyt, "A review of the IEEE 1785 standards for rectangular waveguides above 110 GHz," in *Proc. 89th ARFTG Microw. Meas. Conf. (ARFTG)*, Jun. 2017, pp. 1–4, doi: 10.1109/ARFTG.2017.8000830.

Chad Bartlett (Member, IEEE) was born in Nelson, BC, Canada, in 1987. He received the B.Eng. and M.A.Sc. degrees in electrical engineering from the University of Victoria, Victoria, BC, in 2017 and 2019, respectively, and the Dr.-Ing. degree in electrical engineering from Kiel University, Kiel, Germany, in 2023.

His primary research interests include microwave and millimeter-wave passive components, filters, multiplexers, and antenna networks for the next generation of satellite and communication systems, as well as developing methods for overcoming challenges in microscale designs.

Dr. Bartlett was a member of the European Union's Horizon 2020 Research and Innovation Programme for early-stage researchers where his work focused on advanced filter solutions for high-performance millimeter- and submillimeter-wave systems, from 2019 to 2023.

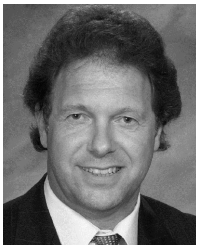

Jens Bornemann (Life Fellow, IEEE) received the Dipl.-Ing. and Dr.-Ing. degrees in electrical engineering from the University of Bremen, Bremen, Germany, in 1980 and 1984, respectively.

From 1984 to 1985, he worked as an Engineering Consultant. In 1985, he joined the University of Bremen, as an Assistant Professor. Since April 1988, he has been with the Department of Electrical and Computer Engineering, University of Victoria, Victoria, BC, Canada, where he became a Professor in 1992. From 1992 to 1995, he was a fellow of the British Columbia Advanced Systems Institute, BC, Canada. In 1996, he was a Visiting Scientist with Spar Aerospace Ltd. (now MDA Space), Sainte-Anne-de-Bellevue, QC, Canada, and a Visiting Professor with the Microwave Department, University of Ulm, Ulm, Germany. From 1997 to 2002, he was a Co-Director of the Center for Advanced Materials and Related Technology (CAMTEC), University of Victoria. In 2003, he was a Visiting Professor with the Laboratory for Electromagnetic Fields and Microwave Electronics, ETH Zürich, Zürich, Switzerland. He has coauthored *Waveguide Components for Antenna Feed Systems—Theory and Design* (Artech House, 1993) and has authored or coauthored more than 400 technical articles. His research activities include RF/wireless/microwave/millimeter-wave components and systems design, and field-theory-based modeling of integrated circuits, feed networks, and antennas.

Dr. Bornemann is a fellow of the Canadian Academy of Engineering (CAE) and the Engineering Institute of Canada (EIC), and serves on the Editorial Advisory Board of the *International Journal of Numerical Modelling*. From 1999 to 2002, he served as an Associate Editor for IEEE TRANSACTIONS ON MICROWAVE THEORY AND TECHNIQUES in the area of microwave modeling and computer-aided design (CAD). From 1999 to 2009, he served on the Technical Program Committee of the IEEE MTT-S International Microwave Symposium. From 2006 to 2008, he was an Associate Editor of the *International Journal of Electronics and Communications*. He is a Registered Professional Engineer in the Province of British Columbia, Canada.

Fynn Kamrath (Graduate Student Member, IEEE) received the B.Sc. and M.Sc. degrees in electrical engineering and information technology from Kiel University, Kiel, Germany, in 2017 and 2019, respectively, where he is currently pursuing the Dr.-Ing. degree with the Chair of Microwave Engineering, Institute of Electrical Engineering and Information Technology.

His research interests include the design, realization, and optimization of center frequency and bandwidth tunable microwave filters.

Michael Höft (Senior Member, IEEE) was born in Lübeck, Germany, in 1972. He received the Dipl.-Ing. degree in electrical engineering and the Dr.-Ing. degree from the Hamburg University of Technology, Hamburg, Germany, in 1997 and 2002, respectively.

From 2002 to 2013, he was with the Communications Laboratory, European Technology Center, Panasonic Industrial Devices Europe GmbH, Lüneburg, Germany. There he was at first a Research Engineer and then the Team Leader, where he had been engaged in the research and development of microwave circuitry and components, particularly filters for cellular radio communications. Then he was at the same organization from 2010 to 2013 the Group Leader of research and development of sensor and network devices. Since October 2013, he has been a Full Professor with the Faculty of Engineering, University of Kiel, Kiel, Germany, where he currently heads the Chair of Microwave Engineering, Institute of Electrical and Information Engineering. His research interests include active and passive microwave components, submillimeter-wave quasi-optical techniques and circuitry, microwave and field measurement techniques, microwave filters, microwave sensors, and magnetic field sensors.

Dr. Höft is a member of the European Microwave Association (EuMA), the Association of German Engineers (VDI), and the German Institute of Electrical Engineers (VDE).